Development and Verification of a Three-Dimensional Multigroup Hybrid Finite Element Diffusion Solver in Cylindrical Geometry for Molten Salt Fast Reactor Analysis

John Caesar Katabarwa[1], Yeon Sang Jung[2], Jooil Yoon[1*]

[1]*KEPCO International Nuclear Graduate School, 658-91 Haemaji-ro, Seosaeng-myeon, Ulju-gun, Ulsan, 45014, Korea*
[2]*Korea Atomic Energy Research Institute, 989-111 Daedeok-daero, Yuseong-gu, Daejeon, 34057, Korea*
[*]*Corresponding author: jiyoon@kings.ac.kr*

**Keywords : hybrid finite element method, cylindrical geometry, molten salt fast reactor, code verification*

1. Introduction

Core analysis of the Molten Salt Fast Reactor (MSFR) is generally carried out in cylindrical coordinates. The core is an open cavity bounded by a curved fuel–blanket interface [1], which a cylindrical formulation represents directly.

The MSFR core is spatially homogeneous and operates in a fast spectrum, so scattering is strongly anisotropic and transport effects pronounced. The hybrid finite element method (HFEM), akin to the variational nodal method [2], suits cores of this kind. A solver of this type has been developed and validated for molten salt reactor transients in PROTEUS-NODAL [3], and the method is implemented in Griffin for spatially homogenized models with pronounced neutron streaming [4].

As a first step toward an HFEM transport capability in cylindrical geometry, a diffusion solver has been developed and verified here as a proof of principle. It is three-dimensional, multigroup, and formulated directly in r–θ–z geometry.

2. Numerical Method

Three implementations are distinguished throughout. The solver reported here is in Mathematica and is the subject of the verification. A second HFEM, in Python, shares no source with it and serves as an internal cross-check; its agreement is discussed in Section 3.1, but none of its results are tabulated here. The finite-difference (FDM) solver, also in Python, shares no formulation, code or author with either, which is what makes it independent. Every k below is from the Mathematica HFEM unless labelled FDM or analytic.

2.1. HFEM weak form for the diffusion equation

HFEM relaxes the continuity requirement of the conventional finite element method: the flux is allowed to be discontinuous across element faces, and continuity is instead enforced weakly, through a Lagrange multiplier defined on each face and equal to the net current there. This makes the discretization conservative on each element, not only in the global sum.

For one energy group, the weak form is written as:

$$(\nabla\varphi^*, D\nabla\varphi)_D + (\varphi^*, \Sigma_a\varphi)_D - (\chi^*, [\varphi])_\Gamma - ([\varphi^*], \chi)_\Gamma + \frac{1}{2}(\varphi^*, \varphi)_{boundary} = (\varphi^*, q)_D \quad (1)$$

where

φ, χ	volumetric flux inside the element, discontinuous across element faces; and the surface multiplier on each interior face, equal to the net current through it
φ^*, χ^*	test functions corresponding to φ and χ
∇	gradient operator
D	diffusion coefficient, $D = 1/(3\Sigma_{tr})$
Σ_a, Σ_{tr}	absorption and transport cross sections. For the multigroup case Σ_a is replaced by the removal cross section $\Sigma_{r,g} = \Sigma_{t,g} - \Sigma_{s,g\to g}$, where g is the energy group index, Σt the total cross section and Σs,g→g the within-group scattering
$\nu\Sigma_f$	fission production cross section
k	multiplication eigenvalue
q	volumetric source, $q = \nu\Sigma_f\varphi/k$. For the multigroup case q_g also collects in-scattering from the other groups
$(\cdot,\cdot)_D$	integration over the element volume D
$(\cdot,\cdot)_\Gamma$	integration over the element faces Γ
$(\cdot,\cdot)_{boundary}$	integration over the part of Γ that lies on the outer boundary
$[\cdot]$	jump across a face, $[f] = f^+ - f^-$
½	half-range factor of the vacuum condition in Marshak form

The first two terms are the leakage and absorption of the element interior; the third and fourth impose weak continuity of the flux, with χ enforcing continuity of the net current; the fifth imposes the vacuum condition on the outer boundary. Requiring this to hold for all φ* and χ* returns the diffusion equation inside the element.

The discretized problem is solved with a response matrix formulation: for given incoming partial currents and volumetric source, the outgoing partial currents on each element face follow as:

$$J_{out} = RJ_{in} + B(E\psi) \quad (2)$$

where

J_{out}, J_{in}	outgoing and incoming partial-current moments on the element faces
R, B	current and source response matrices
E	volumetric mass matrix of the basis
ψ	fission-source coefficient vector, $\psi = \nu\Sigma_f\varphi/k$, so that $E\psi$ is the volumetric source projected onto that basis

The full derivation of the response matrices is given in [2]. Elements are swept in a red–black ordering as the inner iteration.

2.2. Implementation in cylindrical coordinates

Two considerations follow directly from the coordinate system. First, the gradient carries an additional metric factor: the azimuthal derivative in r–θ–z coordinates carries a factor $\frac{1}{r}$, so this factor must be included when the response matrices are formed.

Second, the coordinate singularity at $r = 0$ is treated by removing from the basis any entry that would produce a singular term. Two conditions are imposed: zero radial slope, and no azimuthal dependence, since the azimuthal integrand carries the $\frac{1}{r}$ weight and is otherwise non-integrable at $r = 0$.

The solver checks two admissibility conditions: the degree rule $p_s \le p_v - 2$ and the degree-of-freedom rule $n_V \ge N_f\, n_S$, with n_V and n_S the numbers of volumetric and surface basis functions and N_f the face count. Both are sufficient, not necessary. The setting $p_v/p_s = 1/0$ used throughout Table I satisfies neither, having $n_V = 3$ against $N_f\, n_S = 4$, and is retained because it places one volumetric unknown per cell and so matches a cell-average finite-difference method like for like. A unit spectral radius is what a conservative response matrix is expected to give, so $\rho(R) = 1.000000$ shows only that the sweep does not diverge. The evidence for 1/0 is accuracy: on a bare cylinder with a closed-form solution it converges to the analytic eigenvalue at −59.6, −16.8 and −4.3 pcm for 4, 8 and 16 rings, the O(h2) the 2p law requires. The Table IV pairs satisfy both rules on four faces, from 3/0 ($0 \le 1$, $10 \ge 4$) to 4/2 ($2 \le 2$, $15 \ge 12$).

3. Numerical Results

Four configurations recur through Section 3. The five-region core — inner and outer fuel-salt rings, fertile blanket, shield and wall — is one group on a 20 × 4 mesh, reflecting radially (Tables II and V). The two-region core is one group on 16 cells (Fig. 1, Table III). The MSFR fuel region is zero flux at R = 112.75 cm: one group on 6 rings × 8 sectors, azimuthally uniform (Table IV), 34 groups (Table VII and Fig. 3), and 8 × 4 × 8 in r–θ–z (Fig. 4). Fuel to 112.75 cm plus blanket to 156.3 cm, one group, 8 sectors, is Table VI.

Throughout, Δk is computed from the five-decimal k printed, which resolves about 1 pcm. Table I is referenced to the Richardson-extrapolated FDM limit 0.94979, to the analytic 0.91943 for the bare cylinder and to the FDM on the same mesh for the reflector-wrapped case; Table II to its 3/1 rung; Table V to its Richardson limit; Tables VI and VII to a finer mesh solved for the purpose and not tabulated, 32+16 at k = 1.03951 and 32 × 4 respectively, the latter itself not converged. Neither reference is exact, so the fine-end entries are inflated and the coarse end is the one to read. Every eigenvalue uses $p_v/p_s = 1/0$ unless the table states otherwise, and timings are wall clock on Windows 64-bit, 6 cores, Wolfram 15.0.0, comparable between rungs only.

3.1. Cross-code verification

Comparing HFEM and FDM on the same mesh would mix the HFEM error with the FDM's own, so in Table I every HFEM result is referenced to a converged value. The FDM was extended to multigroup for this work, so the MSFR fuel-region rows are 34-group. The 34-group constants were generated with Serpent 2.2.1 from ENDF/B-VII.1 for the MSFR fuel-salt composition, with 800 000 neutrons per cycle over 300 active cycles. Outers are converged on the L2 norm of the cell-integrated fission-source difference, to 1×10^{-12} for Tables IV and VI and 1×10^{-11} elsewhere, reached in 76–80 of a 300 budget; k is not tested separately, and only Table VII's finest rung stops at that budget. The independently written Python HFEM reproduces the Mathematica eigenvalue on all six cases run, the difference lying below the outer convergence tolerance rather than being resolved by it. Verification here is against an independent solver and closed-form solutions; it is not validation, which would require measurement or an accepted benchmark, and the Monte Carlo results of [3] are the intended validation reference.

Table I: Verification against independent references

Reference	Problem	pv/ps	k (HFEM)	k (FDM)	Δk HFEM / FDM (pcm)
FDM, converged	Fuel region, 8 × 4	1/0	0.94968	0.94656	−11.6 / −340.1
FDM, converged	Fuel region, 16 × 4	1/0	0.94975	0.94903	−4.2 / −80.0
FDM, converged	Fuel region, 32 × 4	1/0	0.94977	0.94962	−2.1 / −17.9
FDM, converged	Fuel region, Richardson	1/0	0.94978	0.94979	−1.1 / 0.0
Analytic	3-D bare cylinder, 8 × 4 × 8	1/0	0.92005	0.91678	+67.4 / −288.2
FDM, same mesh	3-D reflector-wrapped, 8 × 8 × 10	1/0	1.09797	1.09800	−2.7 / 0.0

3.2. Basis (p) refinement

Raising the basis order at fixed mesh resolves the intra-nodal flux without subdividing anything. Moving from p_v=1 to p_v= 2 moves the eigenvalue by 36.3 pcm on the five-region core of Table II at a fixed 20 × 4 mesh: 0.96388 at 1/0 against 0.96423 at 2/0. The accessible orders are limited by the degree rule of Section 2.2, which excludes the higher side orders at low volume

order rather than the low ones; the blank panels of Fig. 1 are those inadmissible pairs.

At 1/0 the eigenvalue is within 37.3 pcm of the 3/1 rung while the worst cell power is 7 % out — a converged eigenvalue is not a converged flux. %ΔP is the RMS and largest cell power error against the reference rung, over the fissile cells only.

Table II: Basis refinement, five-region core

Vol / Surf	k_{eff}	Δk (pcm)	%ΔP RMS	%ΔP MAX
1 / 0	0.96388	−37.3	2.165	6.984
2 / 0	0.96423	−1.0	0.249	0.841
3 / 0	0.96424	0.0	0.000	0.000
3 / 1	0.96424	0.0	0.000	0.000

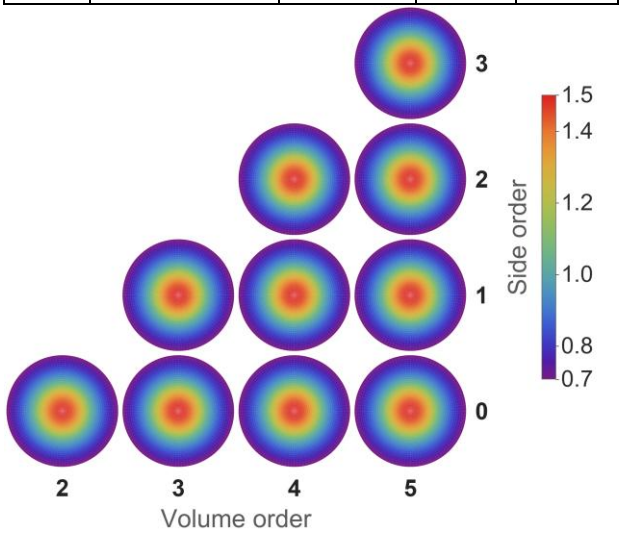


Fig. 1. p-refinement at a fixed 16-cell mesh

Table III: Degrees of freedom and cost

p_V/p_S	n_V	n_S	Vol DOF	Cur DOF	Iters	Build s	Solve s	MB
1/0	3	1	48	64	70	0.73	0.53	0.6
2/0	6	1	96	64	74	3.41	0.58	0.6
3/1	10	2	160	128	76	13.08	0.65	0.7
4/2	15	3	240	192	74	34.70	0.67	0.8
5/3	21	4	336	256	73	76.43	0.82	1.1

Table IV: Effect of the side order

p_V/p_S	k	Δk vs $p_S = 0$	Side DOF per face	Higher-mode share
3/0	1.03711	0.0	1	0.00 %
3/1	1.03711	0.0	2	9.74 %
4/0	1.03711	0.0	1	0.00 %
4/1	1.03711	0.0	2	9.74 %
4/2	1.03711	0.0	3	9.75 %

The eigenvalue is insensitive to the side order even though the higher surface modes carry 9.74 % of the face-current norm. With identical neighbouring sectors the net current per face, which $p_S = 0$ represents exactly, is all the eigenvalue depends on. The claim was tested: an absorber in two of the eight sectors over the outer two rings separates 3/0 from 3/1 by 133.1 pcm, the higher-mode share rising to 13.79 %. So $p_S = 0$ is justified for azimuthally smooth problems, not in general. The identical k on all five rungs of Table IV is that result; the higher-mode share is the face-current norm above the flat mode, zero by construction at $p_S = 0$.

3.3. Mesh (h) refinement

Subdividing the mesh at fixed basis order converges the eigenvalue monotonically, and considerably faster than the flux shape; Table VI shows both on the same rung: at 8+4 the eigenvalue is 25.0 pcm from the reference while the cell-integrated flux is still 0.88 % out in L2 norm. On the 34-group fuel region of Table VII the eigenvalue is within 2.1 pcm of its limit at 16 × 4. Table VI's norms use cell-integrated flux normalised to unit total, each coarse cell against the fine cells it contains, and its two constants are representative, matched to MSFR reactivity rather than taken from the delivered set. Each region carries a whole number of equal cells, so the fuel/blanket interface falls on a cell face at every rung and the coarse-end order is not an alignment artefact. The solution stays smooth through the axis with no special treatment there (Fig. 2, k = 1.72377), a synthetic one-group disc with $\nu\Sigma_f/\Sigma_r = 2.0$, radius 4 and 4 rings × 8 sectors.

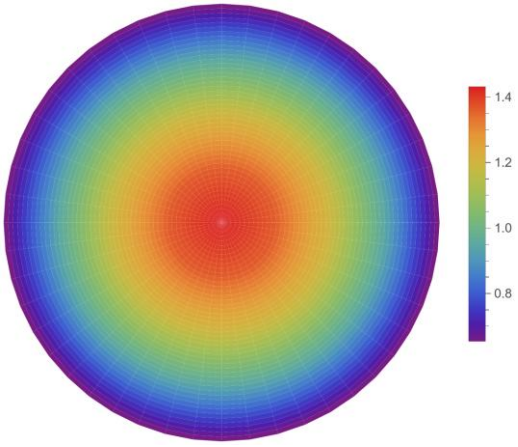


Fig. 2. Centre-peaked flux on a vacuum-bounded disc

Each region is refined by one, two, four and eight, so the ratio is constant and Richardson extrapolation applies; the 20 × 4 mesh matches the limit to the precision shown. Where no closed form exists, the sequence is referenced to its own Richardson extrapolation, following [5]; that limit is an estimate, not a benchmark.

Table V: Mesh refinement and the Richardson limit

Mesh	k_{eff}	Δk vs Richardson (pcm)
5 × 4	0.96421	−3.1
10 × 4	0.96424	0.0
20 × 4	0.96424	0.0
40 × 4	0.96424	0.0

Table VI: Flux-shape convergence

Fuel + blanket	k	L2 (×10⁻³)	L∞ (×10⁻³)	rel %	Order	Δk (pcm)
2+1	1.03781	1.95	2.73	4.16	—	−163.5
4+2	1.03874	0.58	1.04	2.36	1.751	−74.1
8+4	1.03925	0.11	0.239	0.88	2.396	−25.0
16+8	1.03945	0.0128	0.0303	0.20	3.111	−5.8

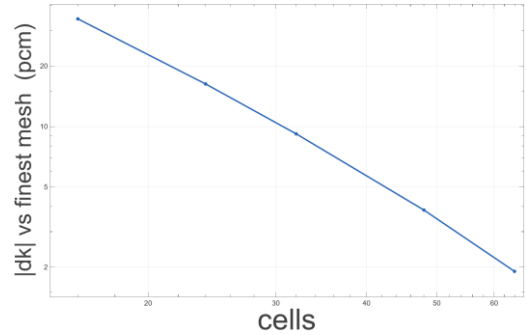


Fig. 3. h-refinement error against the finest mesh

Table VII: Mesh refinement, 34-group fuel region

Mesh	keff	Δk (pcm)	Time (s)
4 × 4	0.94944	−34.7	91.0
6 × 4	0.94961	−16.8	173.8
8 × 4	0.94968	−9.5	278.0
12 × 4	0.94973	−4.2	536.1
16 × 4	0.94975	−2.1	1249.2
32 × 4	0.94977	0.0	13795.1

3.4. Three-dimensional verification

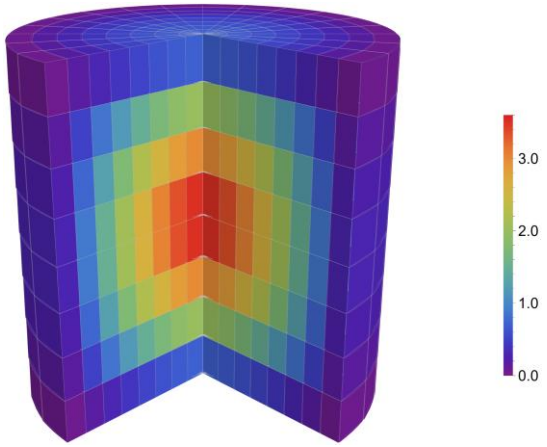


Fig. 4. Scalar flux in the MSFR fuel region

In three dimensions the FDM, also written for r–θ–z, is again the independent check. The degree-of-freedom rule tightens on six faces: at 1/0 the element carries n_V = 4 against $N_f\, n_S$ = 6, so it is not satisfied here either; the justification is again the agreement below. On a bare cylinder with an analytic solution, at 8 × 4 × 8, the HFEM returns k = 0.92005 against the analytic 0.91943 (+67.4 pcm) and the FDM 0.91678 (−288.2 pcm); the two straddle it, as a response-matrix method and a cell-average method should on a coarse mesh. The intended configuration is a fuel cylinder in a reflector annulus, capped at each end, every outer face vacuum, so both leakages are live. On that problem the like-for-like comparison at p_v = 1, one volumetric unknown per cell, agrees with the FDM to 2.7 pcm (1.09797 against 1.09800) on 8 × 8 × 10 = 640 cells. Raising the basis to p_v = 2 moves the HFEM away from the FDM by 144.4 pcm, as it should: the added order resolves intra-nodal curvature a cell-average method cannot represent. Fig. 4 shows the fuel region itself, not that bare cylinder, its colours the cell-average flux at volume-weighted mean unity, peak 3.52.

4. Conclusion

We have verified a three-dimensional multigroup HFEM diffusion solver formulated directly in cylindrical geometry, in which the axis singularity is removed by a constraint on the basis rather than by a cut-off radius or a special case in the sweep.

Referenced to a converged finite-difference limit, the eigenvalue error falls from 11.6 pcm on a 32-cell mesh to below the 1.1 pcm the five-decimal k resolves, under extrapolation, where the finite-difference error is 340.1 pcm — roughly thirty times more accurate at equal mesh, accuracy per cell rather than per degree of freedom, since at 1/0 the element carries three volumetric moments against the FDM's one.

The present implementation is limited in two respects we intend to address: the sweep carries no coarse-mesh acceleration, so its iteration count grows under mesh refinement, and the P_1 closure carries scattering anisotropy through the average cosine alone.

ACKNOWLEDGEMENT

This research was supported by the 2026 Research Fund of the KEPCO International Nuclear Graduate School (KINGS), the Republic of Korea.

REFERENCES

[1] M.K. Jaradat, G. Yang, H. Park, W.S. Yang, C.H. Lee, Y.S. Jung, Multiphysics Coupling of PROTEUS-NODAL and SAM for Molten Salt Reactor Simulation, Argonne National Laboratory Report ANL/NSE-20/7, 2020.
[2] T. Zhang, Z. Li, Variational nodal methods for neutron transport: 40 years in review, Nucl. Eng. Technol., Vol. 54, No. 9, pp. 3181–3204, 2022.
[3] M.K. Jaradat, H. Park, W.S. Yang, C. Lee, Development and validation of PROTEUS-NODAL transient analyses capabilities for molten salt reactors, Ann. Nucl. Energy, Vol. 160, 108402, 2021.
[4] Y. Wang, Z.M. Prince, H. Park, et al., Griffin: A MOOSE-based reactor physics application for multiphysics simulation of advanced nuclear reactors, Annals of Nuclear Energy, Vol. 211, 110917, 2025.
[5] K.F. Hansen, C.M. Kang, Finite element methods in reactor physics analysis, Advances in Nuclear Science and Technology, Vol. 8, pp. 173–253, 1975.